Regenerative Therapy 24 (2023) 592–601

Contents lists available at ScienceDirect

Regenerative Therapy

journal homepage: http://www.elsevier.com/locate/reth

Original Article

Non-apoptotic regulated cell death in Fuchs endothelial corneal dystrophy

Saki Sakakura [a], Emi Inagaki [a, b, c, **], Tomoko Sayano [a, d], Risa Yamazaki [a], Noemi Fusaki [e, ***], Shin Hatou [a, d], Masatoshi Hirayama [a], Kazuo Tsubota [a], Kazuno Negishi [a], Hideyuki Okano [b], Shigeto Shimmura [a, f, *]

[a] Department of Ophthalmology, Keio University School of Medicine, 35 Shinanomachi, Shinjuku, Tokyo 160-8582, Japan
[b] Department of Physiology, Keio University School of Medicine, 35 Shinanomachi, Shinjuku, Tokyo 160-8582, Japan
[c] Japan Society for the Promotion of Science, 5-3-1 Kojimachi, Chiyoda, Tokyo 102-0083, Japan
[d] Cellusion Inc. 8-6 Nihonbashi-Kobunacho, Chuo-ku, Tokyo 103-0024, Japan
[e] University of Tokyo Pandemic Preparedness, Infection and Advanced Research Center, 4-6-1 Shirokanedai, Minato, Tokyo 108-8639, Japan
[f] Department of Clinical Regenerative Medicine, Fujita Medical Innovation Center, Fujita Health University, Haneda Innovation City Zone A, 1-1-4, Hanedakuko, Ota-ku, Tokyo 144-0041, Japan

ARTICLE INFO

Article history:
Received 23 September 2023
Received in revised form
15 October 2023
Accepted 5 November 2023

Keywords:
Cell death
Fuchs' endothelial corneal dystrophy
Induced pluripotent stem cells
Oxidative stress
Parthanatos
Mitochondria

ABSTRACT

Introduction: Fuchs endothelial corneal dystrophy (FECD) is the leading cause of corneal blindness in developed countries. Corneal endothelial cells in FECD are susceptive to oxidative stress, leading to mitochondrial dysfunction and cell death. Oxidative stress causes many forms of cell death including parthanatos, which is characterized by translocation of apoptosis-inducing factor (AIF) to the nucleus with upregulation of poly (ADP-ribose) polymerase 1 (PARP-1) and poly (ADP-ribose) (PAR). Although cell death is an important aspect of FECD, previous reports have often analyzed immortalized cell lines, making the evaluation of cell death difficult. Therefore, we established a new *in vitro* FECD model to evaluate the pathophysiology of FECD.

Methods: Corneal endothelial cells were derived from disease-specific induced pluripotent stem cells (iPSCs). Hydrogen peroxide (H_2O_2) was used as a source for oxidative stress to mimic the pathophysiology of FECD. We investigated the responses to oxidative stress and the involvement of parthanatos in FECD-corneal endothelial cells.

Results: Cell death ratio and oxidative stress level were upregulated in FECD with H_2O_2 treatment compared with non-FECD control, indicating the vulnerability of oxidative stress in FECD. We also found that intracellular PAR, as well as PARP-1 and AIF in the nucleus were upregulated in FECD. Furthermore, PARP inhibition, but not pan-caspase inhibition, rescued cell death, DNA double-strand breaks, mitochondrial membrane potential depolarization and energy depletion, suggesting that cell death was mainly due to parthanatos.

Conclusions: We report that parthanatos may be involved in the pathophysiology of FECD and targeting this cell death pathway may be a potential therapeutic approach for FECD.

1. Introduction

The corneal endothelium plays a critical role in maintaining the corneal transparency [1]. Unlike endothelial cells in other tissues, corneal endothelial cells (CECs) do not proliferate after birth [2]. Loss of endothelial density leads to loss of corneal clarity, resulting in visual impairment. Fuchs endothelial corneal dystrophy (FECD) is characterized by progressive loss of CECs and abnormal extracellular matrix deposition [3], and is one of the most common corneal

* Corresponding author. Department of Ophthalmology, Keio University School of Medicine, 35 Shinanomachi, Shinjuku, Tokyo 160-8582, Japan.
** Corresponding author. Department of Ophthalmology, Keio University School of Medicine, 35 Shinanomachi, Shinjuku, Tokyo 160-8582, Japan.
*** Corresponding author.
E-mail addresses: eminagaki512@keio.jp (E. Inagaki), naomisas@gmail.com (N. Fusaki), shigeto.shimmura@fujita-hu.ac.jp (S. Shimmura).
Peer review under responsibility of the Japanese Society for Regenerative Medicine.

https://doi.org/10.1016/j.reth.2023.11.001

Abbreviations:

CECs	corneal endothelial cells
FECD	Fuchs endothelial corneal dystrophy
PARP-1	poly (ADP-ribose) polymerase-1
PAR	poly (ADP-ribose)
AIF	apoptosis-inducing factor
iPSCs	induced pluripotent stem cells
PBMC	peripheral blood mononuclear cells
EFSC	eye field stem cells
NCSC	neural crest stem cells
FBS	fetal bovine serum
γH2AX	phospho-histone H2AX
PBS	phosphate-buffered saline
NAC	N-acetylcysteine
Z-VAD-FMK	z-VaD-Ala-Asp-fluoromethylketone
H_2O_2	hydrogen peroxide
ROS	reactive oxidative stress
MMP	mitochondrial membrane potential
FECD-JPN	a Japanese FECD patient
FECD-EUR	a European Caucasian FECD patient
CTRL	a healthy Japanese volunteer as a control
CDH2	cadherin 2
ATP1A1	Na/K ATPase α-1
HO-1	heme oxygenase 1
NRF2	nuclear factor-erythroid 2-related factor 2
SOD2	superoxidase dismutase 2
TXNRD1	thioredoxin reductase 1
NAMPT	nicotinamide phosphoribosyltransferase

endothelial diseases worldwide [4]. Since the typical age of onset of FECD is over 50 years old and the prevalence is increasing with age, the number of patients is expected to increasing in the future [5].

FECD is caused by both environmental and genetic factors [3,6]. Cellular stress, such as oxidative stress [6–8] and endoplasmic reticulum (ER) stress [9], contributes to the pathogenesis of FECD by inducing mitochondrial dysfunction [10,11], endothelial-mesenchymal transition [12] and cell death [13]. Oxidative stress has received particular attention, and antioxidant therapy is a promising candidate for the treatment of FECD [7,8,12,14]. Mechanisms of oxidative stress-induced endothelial cell death in FECD have been reported to involve several types of cell death [15], including apoptosis [13,16] and ferroptosis [17]. However, because cell death in FECD progresses very slowly with aging, we hypothesized that the mechanism may be similar to the cell death caused by metabolic changes due to aging seen in neurodegenerative diseases.

Parthanatos, proposed in 2009 by Dawson et al. [18,19], is a non-apoptotic regulated cell death induced by energy depletion seen in neurodegenerative diseases [20]. In parthanatos, overexpression of poly (ADP-ribose) polymerase 1 (PARP-1) and poly (ADP-ribose) (PAR) polymers overexpression, translocation of apoptosis-inducing factor (AIF) translocation into the nucleus and energy depletion such as NAD^+ and ATP are the key findings [21,22]. PAR-AIF interaction and NAD^+ depletion lead to depolarization of the mitochondrial membrane [23]. AIF then translocates to the nucleus, where it induces extensive DNA fragmentation and cell death [24].

In FECD, cell death is an essential aspect that could be a target for potential new drugs. To date, established cell lines have been used to study the etiology of FECD because of the ease of culturing cells [9,12,25]. However, an immortalized cell line may not be suitable to evaluate the precise mechanisms of cell death. In order to overcome this drawback, we established a new *in vitro* FECD model by inducing CECs from disease-specific induced pluripotent stem cells (iPSCs) [26]. FECD has ethnic diversity in prevalence, onset and genetic factors [3,27,28]. Therefore, we generated disease-specific iPSCs from a Japanese and a Caucasian European FECD patient and examined the effect of oxidative stress on each iPS-derived CEC to reveal the contribution of parthanatos in FECD.

2. Methods

2.1. Generation of disease-specific iPSCs

As described previously [29], we induced iPSCs from peripheral blood mononuclear cells (PBMCs). Briefly, PBMCs were obtained from two FECD patients (72-year-old Japanese female and 64-year-old European Caucasian female) and one healthy subject (68-year-old Japanese male). PBMCs were separated on a Ficoll-paque PREMIUM (GE Healthcare, Chicago, USA) gradient, and T cells were isolated with anti-CD3 monoclonal antibody (BD Biosciences, New Jersey, USA) and rIL-2 contained GT-T502 medium (Kohjin Bio Co., Ltd., Saitama, Japan). On day 6, T cells were infected with a Sendai virus vector carrying OCT3/4, SOX2, KLF4, and c-MYC. Two days after infection, cells were harvested and transferred to a 10 cm dish with mitomycin C-treated SNL feeder cells at 5×10^4 cells/dish. After 24 h, the medium was changed to human iPSC medium. The medium was changed every other day until the colonies were picked on day 25. Established iPSCs were maintained in a feeder-free condition in StemFit AK02 N (Reprocell, Kanagawa, Japan) on iMatrix-511 silk (Nippi, Tokyo, Japan) coated 6-well plates. The medium was changed every 1–2 days, and cells were passaged with TrypLE Select (Thermo Fisher, Massachusetts, USA) every seven days. All experimental procedures were approved by the Keio University School of Medicine Ethics Committee (approval number: 20130221).

2.2. Differentiation of disease-specific iPSCs into CECs

To differentiate CECs from iPSCs, we modified a previously published protocol by Zhao [30]. After iPSCs reached 80 % confluence in culture, the medium was switched to eye field stem cell (EFSC) medium. EFSC medium included DMEM/F12 (Nacalai Tesque, Inc., Kyoto, Japan) with 1x N2 (R&D Systems, Inc., Minnesota, USA), 1x B27 (Thermo Fisher, Massachusetts, USA), 0.2 % BSA (FUJIFILM Wako Pure Chemical Corp., Osaka, Japan), 2 mM L-ala-L-glutamine (Sigma-Aldrich Co. Llc., Missouri, USA), 0.1 mM MEM nonessential amino acids (Sigma-Aldrich Co. Llc., Missouri, USA), 0.1 mM 2-mercaptoethanol (Thermo Fisher, Massachusetts, USA) and 20 ng/ml bFGF (PeproTech, Inc., New Jersey, USA) for one day. For the following six days, cells were cultured in EFSC medium supplemented with 5 μM SB431542 (Sigma-Aldrich Co. Llc., Missouri, USA), 50 nM LDN193189 (Reprocell, Kanagawa, Japan) and 1 μM IWP2 (Sigma-Aldrich Co. Llc., Missouri, USA). The medium was changed every day. Cells were dissociated with TrypLE Select and passaged in Neural Crest Stem Cells (NCSC) medium on iMatrix-511 silk coated 6-well plates. NCSC medium included DMEM/F12 and Neurobasal plus medium (Thermo Fisher, Massachusetts, USA) (50:50) with 1x N2, 1x B27, 0.3 mM 2-phospho-L-ascorbic acid (Sigma-Aldrich Co. Llc., Missouri, USA) and 3 mM CHIR 99021 (Tocris Bioscience, Bristol, UK). On the passage day, 10 μM Y-27632 (Nacalai Tesque, Inc., Kyoto, Japan) was also

supplemented. The medium was changed every other day. Seven days later, cells were dissociated with TrypLE Select and passaged in corneal endothelial cell (CEC) medium on 6-well plates coated with FNC Coating Mix (Athena Enzyme Systems, Maryland, USA). CEC medium included human endothelial SFM (Thermo Fisher, Massachusetts, USA) with 5 % fetal bovine serum (FBS) (Nichirei Bioscience Inc., Tokyo, Japan), 0.3 mM 2-phospho-L-ascorbic acid, 1 μM SB431542 and 3 μM Y-27632. CEC medium was changed every other day. CECs were passaged every seven days, and cells at passage numbers between 1 and 3 were used for the experiments. Induced cells were observed with phase-contrast microscopy (BIOREVO BZ-9000; KEYENCE Corp., Osaka, Japan).

2.3. Immunostaining and phospho-histone H2AX (γH2AX) expression assay

Cells in 35 mm dishes were fixed with 4 % paraformaldehyde (Nacalai Tesque, Inc., Kyoto, Japan) at room temperature for 10 min and washed with phosphate-buffered saline (PBS). They were blocked in 10 % normal donkey serum with 0.1 % Triton X-100 (Nacalai Tesque, Inc., Kyoto, Japan) for 30 min at room temperature. Samples were incubated with the indicated primary antibodies (Supplementary Table 1) overnight at 4 °C. Cells were washed with PBS and incubated with anti-mouse or anti-rabbit Alexa Fluor 488/555 conjugated secondary IgG antibodies (1:200, anti-mouse Alexa Fluor 488: A-21202, anti-rabbit Alexa Fluor 488: A-21206, anti-rabbit Alexa Fluor 555: A-31572, Thermo Fisher, Massachusetts, USA) and Hoechst 33342 (1:1000, 346–07951, Dojindo Laboratories Co., Ltd., Kumamoto, Japan) for 1 h at room temperature. Cells were washed again with PBS and mounted. Samples were observed with a fluorescent microscope (Axio Imager; Carl Zeiss Inc., Weimar, Germany). For the assessment of phospho-histone H2AX (γH2AX) staining, four images per dish were captured under the same threshold. γH2AX foci and nuclei were counted with Image J [31].

2.4. Quantitative real-time PCR

Total RNA was collected from cultured cells with the RNeasy kit (Qiagen, Hilden, Germany), and cDNA was prepared with the ReverTra Ace α kit (Toyobo Co. Ltd., Osaka, Japan) according to the manufacturer's protocol. Quantitative real-time PCR was performed using Thunderbird SYBR qPCR mix (Toyobo Co. Ltd., Osaka, Japan) on the StepOnePlus Real-Time PCR system (Thermo Fisher, Massachusetts, USA). Primer pairs are described in Supplementary Table 2.

2.5. Cell viability assay

CECs were cultured on 96-well plates coated with FNC Coating Mix at 1×10^4 cells/well until they reached 80 % confluency. Subsequently, they were treated in the presence or absence of 50 μM N-acetylcysteine (NAC) (Sigma-Aldrich Co. Llc., Missouri, USA) in DMSO (Nacalai Tesque, Inc., Kyoto, Japan) or 1 μM PJ34 (MedChem Express, New Jersey, USA) in DMSO or 1 μM z-VaD-Ala-Asp-fluoromethyl ketone (Z-VAD-FMK) (Selleck Chemicals, Texas, USA) in DMSO in CEC medium in the absence of SB431542 and FBS. These reagents were extracted for the accurate analysis of cell viability. Twenty-four hours later, the medium was replaced with hydrogen peroxide (H_2O_2) (FUJIFILM Wako Pure Chemical Corp., Osaka, Japan) at indicated concentrations in CEC medium in the absence of SB431542 and FBS for 4 h. After removal of the medium, cells were stained with 50 nM Sytox Green (Thermo Fisher, Massachusetts, USA) and 1 μg/ml Hoechst 33342 in 100 μl DMEM/F12 without Phenol Red liquid (Nacalai Tesque, Inc., Kyoto, Japan) for 10 min. Images of six fields in a well were captured automatically with In Cell Analyzer 6000 (GE Healthcare, Chicago, USA). Analysis with In Cell Developer Toolbox v1.9 (GE Healthcare, Chicago, USA) was performed, identifying Hoechst 33342 positive nucleus and Sytox Green positive nucleus. The number of Hoechst 33342 and Sytox Green positive cells were counted respectively. The ratio of Sytox Green positive nucleus to Hoechst 33342 positive nuclei was calculated.

2.6. Reactive oxidative stress (ROS) level analysis

Induced CECs were seeded on 96-well plates coated with FNC Coating Mix at 1×10^4 cells/well. They were treated with or without 50 μM NAC in CEC medium in the absence of SB431542 and FBS for 24 h. The medium was replaced with or without 600 μM H_2O_2 in CEC medium in the absence of SB431542 and FBS for 4 h. Intracellular ROS level was evaluated with CellROX green reagent (C10444; Thermo Fisher, Massachusetts, USA). Cells were stained with 5 μM CellROX reagent in CEC medium at 37 °C for 30 min. Images of four fields in a well were captured automatically with a confocal microscope (Cell Voyager CQ1; Yokogawa Electric Co. Ltd., Tokyo, Japan). Total green fluorescent intensity was measured with CellPathfinder (Yokogawa Electric Co. Ltd., Tokyo, Japan).

2.7. Western blotting

Protein samples from the whole cells were extracted with RIPA buffer (Nacalai Tesque, Inc., Kyoto, Japan) supplemented with 1 % Phosphatase inhibitor Cocktail (Nacalai Tesque, Inc., Kyoto, Japan) and 1 % Protease inhibitor Cocktail (Nacalai Tesque, Inc., Kyoto, Japan). Proteins from the nuclear or cytoplasm fractions were extracted with NE-PER Nuclear and Cytoplasmic Extraction Reagents (Thermo Fisher, Massachusetts, USA) according to the manufacturer's protocol. Protein sample volumes were estimated with the TaKaRa BCA Protein Assay Kit (Takara Bio Inc., Shiga, Japan). Proteins were subjected to SDS-PAGE and transferred on a polyvinylidene difluoride membrane (BIO-RAD Laboratories Inc., California, USA). The membranes were blocked with Blocking One (Nacalai Tesque, Inc., Kyoto, Japan) and incubated with primary antibodies: anti-PARP-1 (1:1000, ab32138, Abcam, Cambridge, UK), anti-AIF (1:1000, ab32516, Abcam, Cambridge, UK), anti-Histone H3 (1:1000, ab1791, Abcam, Cambridge, UK), anti-PAR (1:1000, ALX-804-220-R100, Enzo life Sciences, Inc., Exeter, UK), and anti-β-actin (1:1000, ab160639, Abcam, Cambridge, UK) at 4 °C overnight. Incubation was followed with horseradish peroxidase-conjugated anti-rabbit secondary antibody (1:5000, #7074, Cell Signaling Technology, Massachusetts, USA) or anti-mouse secondary antibody (1:3000, #7076, Cell Signaling Technology, Massachusetts, USA) at room temperature for 1 h. Antibody-antigen complexes were detected with SuperSignal West Pico PLUS (Thermo Fisher, Massachusetts, USA) using a CCD camera system (ImageQuant LAS 4000, GE Healthcare, Chicago, USA). The images of uncropped gels are shown in Supplementary Fig. 1. Quantification was performed using Image J [31].

2.8. Mitochondrial membrane potential (MMP) assay

CECs were cultured on 96-well plates coated with FNC Coating Mix at 1×10^4 cells/wells and treated with or without 1 μM PJ34 in CEC medium in the absence of SB431542 and FBS for 24 h. The medium was replaced with or without 600 μM H_2O_2 in CEC medium in the absence of SB431542 and FBS for 4 h. They were stained with JC-10 solution according to the manufacturer's instructions (Cell Meter JC-10 Mitochondrion Membrane Potential Assay Kit; AAT Bioquest, California, USA). Images of four fields in a well were captured automatically with a confocal microscope (Cell Voyager

CQ1). JC-10 exists as a polymer in the mitochondria under high MMP states, while it is released from the mitochondria to the cytoplasm as a monomer under low MMP. Fluorescent intensity of green from the monomer and red from the polymer was analyzed with CellPathfinder. The ratio of red to green fluorescence intensity was calculated.

2.9. Intracellular ATP level measurement

The intracellular ATP level was measured by "Cell no" ATP assay reagent Ver.2 (FUJIFILM Wako Pure Chemical Corp., Osaka, Japan) according to the manufacturer's protocol. CECs were cultured on 96-well plates coated with FNC Coating Mix at 1×10^4 cells/well. They were treated with or without 1 μM PJ34 in CEC medium in the absence of SB431542 and FBS for 24 h. The medium was replaced with or without 600 μM H_2O_2 in CEC medium without SB431542 and FBS for 4 h. ATP reagent was added. Cells were incubated at room temperature for 10 min and luminescence was measured.

2.10. Intracellular NAD^+ level measurement

CECs cultured on 96-well plates coated with FNC Coating Mix at 1×10^4 cells/well were treated with or without 1 μM PJ34 in CEC medium in the absence of SB431542 and FBS for 24 h. The medium was replaced with or without 600 μM H_2O_2 in CEC medium in the absence of SB431542 and FBS for 4 h. The intracellular NAD^+ level was quantified using NAD/NADH-Glo Assay (Promega Corporation, Wisconsin, USA) according to the manufacturer's protocol, and was assessed by measuring luminescence. This assay detects the total content of NAD/NADH. However, the NADH concentration in cells is less than 10 %. Therefore, it is assumed that NAD^+ is the primary component measured in this assay.

2.11. Statistical analysis

Statistical analysis was performed with GraphPad Prism 9.0 (GraphPad Software). The values are the mean ± SD. All experiments have more than three samples in each experiment. One-way analysis of variance (ANOVA) followed by the Bonferroni test was performed to compare three or more groups. For cell death assay of H_2O_2 dose dependency, two-way ANOVA followed by Turkey's test and Steel-Dwass multiple test were used. $P < 0.05$ was considered statistically significant: $^*P < 0.05$, $^{**}P < 0.01$, $^{***}P < 0.001$.

3. Results

3.1. Characteristics of disease-specific iPSC-derived CECs

We successfully established iPSCs lines from a Japanese FECD patient (FECD-JPN), a European Caucasian FECD patient (FECD-EUR) and a healthy Japanese volunteer as a control (CTRL). All iPSC lines expressed pluripotent markers OCT4, SOX2 and NANOG (Fig. 1A). We induced corneal endothelial cells according to a modified protocol first reported by Zhao [30] (Fig. 1B). Induced cells exhibited hexagonal morphology and expressed several CEC markers such as ZO-1, Cadherin 2 (CDH2), and Na/K ATPase α-1 (ATP1A1) (Fig. 1C).

3.2. Reactive oxidative stress in FECD

To examine if the induced CECs exhibited vulnerability to ROS, we treated cells with H_2O_2 (Fig. 2A). The mRNA levels of the antioxidant enzymes heme oxygenase 1 (*HO-1*), nuclear factor-erythroid 2-related factor 2 (*NRF2*), superoxidase dismutase 2 (*SOD2*), and thioredoxin reductase 1 (*TXNRD1*) did not change in

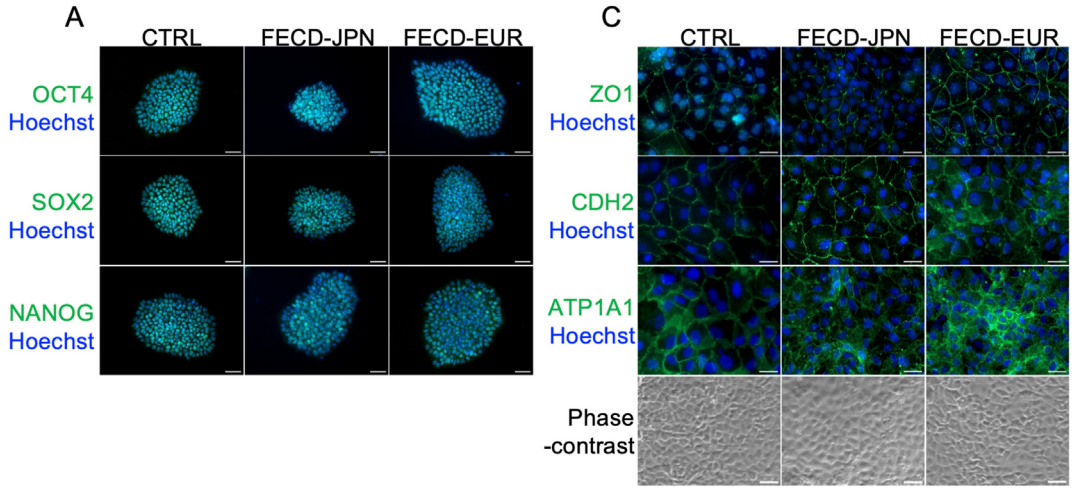

B

Corneal Endothelial Cells differentiation protocol						
	iPSCs	Eye Field Stem Cells		Neural Crest Stem Cells	Corneal Endothelial Cells	
Days	0	7	9	15	22	23
Medium	AK02 medium	EFSC medium	EFSC medium +Supplements	NCSC medium		CEC medium
Scaffold	i-Matrix 511 Silk				FNC Coating Mix	

Fig. 1. Corneal endothelial cells (CECs) induction from iPSCs. (A) Immunostaining of iPSCs for pluripotency markers (OCT4, SOX2, NANOG). Scale bars are 50 μm. (B) Corneal endothelial cell differentiation protocol. (C) Immunostaining of induced cells for corneal endothelial markers (tight junction ZO1, CDH2, ATP1A1) and phase-contrast images. The cells exhibited hexagonal shape. Scale bars are 30 μm in immunostaining images and 30 μm in the phase-contrast images.

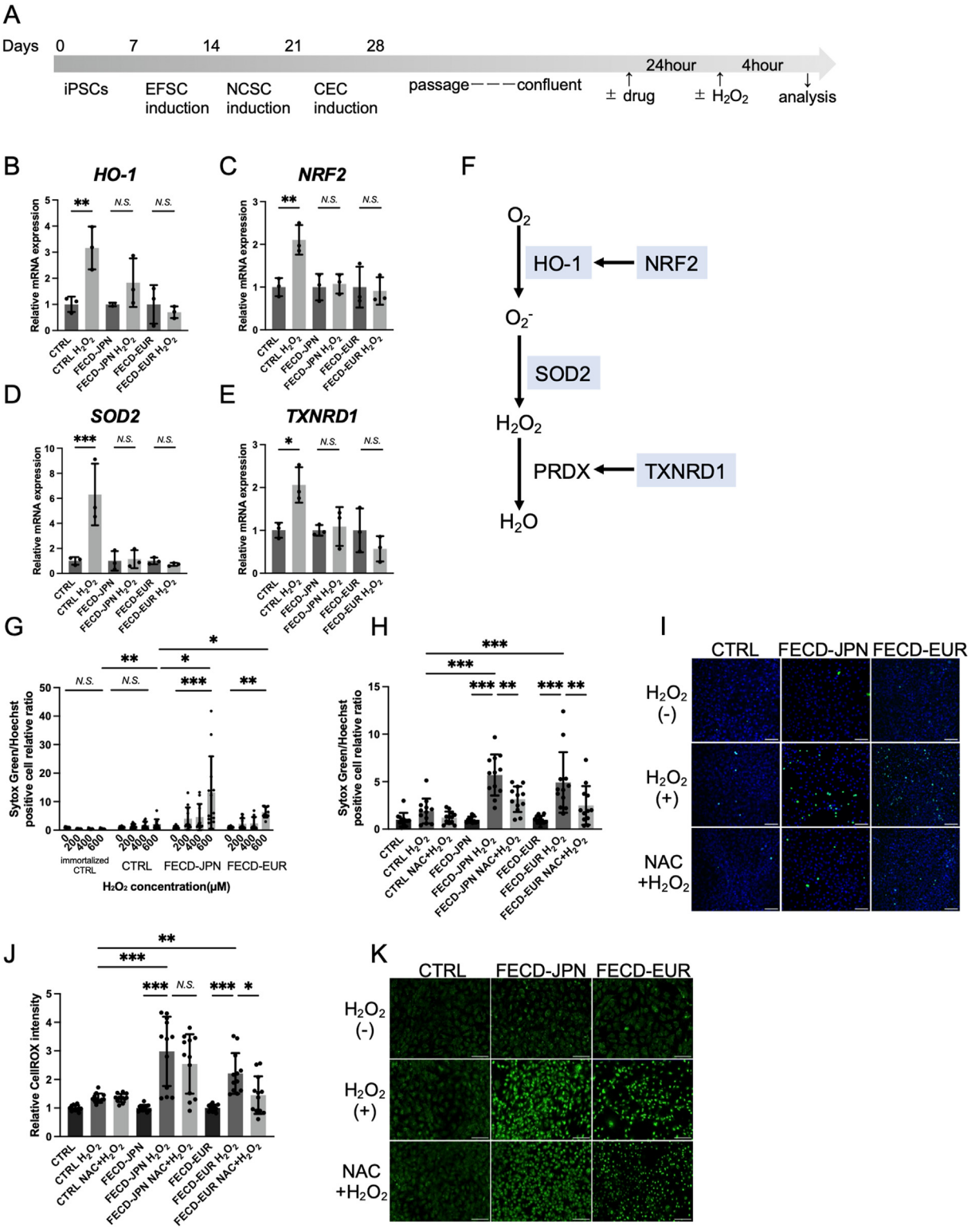

Fig. 2. Vulnerability to reactive oxidative stress (ROS) in FECD. (A) Protocol to assess phenotypes of induced corneal endothelial cells under oxidative stress. (B) Relative mRNA level of *HO-1* after H_2O_2 treatment in each group ($n = 3$, $^{**}p = 2.9 \times 10^{-3}$). (C) Relative mRNA level of *NRF2* after H_2O_2 treatment in each group ($n = 3$, $^{**}p = 4.1 \times 10^{-3}$). (D) Relative mRNA level of *SOD2* after H_2O_2 treatment in each group ($n = 3$, $^{***}p = 2.3 \times 10^{-4}$). (E) Relative mRNA level comparison of *TXNRD1* after H_2O_2 treatment in each group ($n = 3$, $^{*}p = 0.01$). (F) Schematic diagram of the redox pathway. (G) Relative cell death ratio with various concentrations of H_2O_2 in each group ($n = 12$, FECD-JPN H_2O_2 0 μM vs FECD-JPN H_2O_2 600 μM $^{***}p = 4.3 \times 10^{-13}$, FECD-EUR H_2O_2 0 μM vs FECD-EUR H_2O_2 600 μM $^{**}p = 2.6 \times 10^{-3}$, immortalized CTRL H_2O_2 600 μM vs CTRL H_2O_2 600 μM $^{**}p = 7.6 \times 10^{-3}$, CTRL H_2O_2 600 μM vs FECD-JPN H_2O_2 600 μM $^{*}p = 0.03$, CTRL H_2O_2 600 μM vs FECD-EUR H_2O_2 600 μM $^{*}p = 0.03$). (H, I) Relative cell death ratio by H_2O_2 supplemented with NAC in each group ($n = 12$, FECD-JPN vs FECD-JPN H_2O_2 $^{***}p = 1.5 \times 10^{-9}$, FECD-JPN H_2O_2 vs FECD-JPN NAC + H_2O_2 $^{**}p = 1.7 \times 10^{-3}$, FECD-EUR vs FECD-EUR H_2O_2 $^{***}p = 3.8 \times 10^{-7}$, FECD-EUR H_2O_2 vs FECD-EUR NAC + H_2O_2 $^{**}p = 3.4 \times 10^{-3}$, CTRL H_2O_2 vs FECD-JPN H_2O_2 $^{***}p = 8.9 \times 10^{-7}$, CTRL H_2O_2 vs FECD-EUR H_2O_2 $^{***}p = 1.3 \times 10^{-4}$). Sytox Green positive nuclei indicate dead cells. Scale bars are 100 μm. (J, K) Relative ROS level by H_2O_2 supplemented with NAC in each group and representative images ($n = 12$, CTRL H_2O_2 vs FECD-JPN H_2O_2

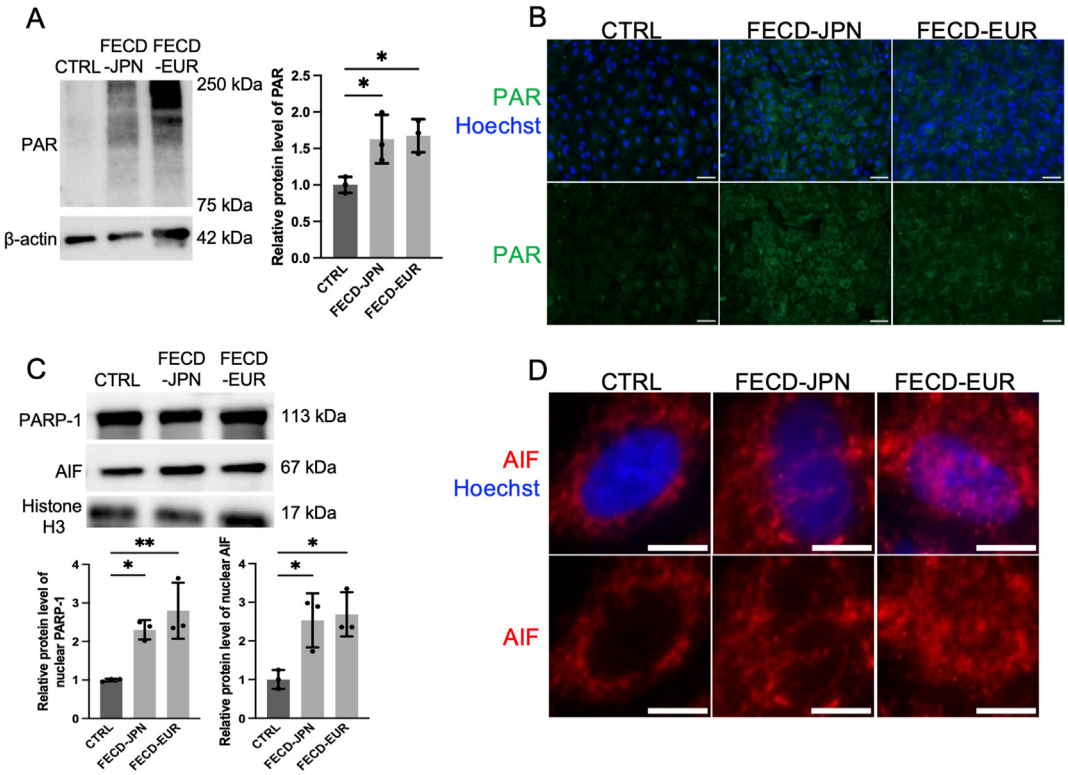

Fig. 3. Upregulation of parthanatos-related molecules in FECD. (A) Relative protein level of PAR polymers ($n = 3$, CTRL = 1, CTRL vs FECD-JPN $*p = 0.04$, CTRL vs FECD-EUR $*p = 0.03$). (B) Immunofluorescent analysis of PAR polymers. Scale bars are 50 μm. (C) Relative protein level of PARP-1 and AIF in the nucleus ($n = 3$, CTRL = 1, PARP-1: CTRL vs FECD-JPN $*p = 0.02$, CTRL vs FECD-EUR $**p = 5.1 \times 10^{-3}$, AIF: CTRL vs FECD-JPN $*p = 0.03$, CTRL vs FECD-EUR $*p = 0.02$). (D) Immunofluorescent analysis of nuclear AIF. Scale bars are 10 μm. All data are presented as the mean ± SD values. All experiments were repeated 3 times independently.

FECD, while a significant upregulation was observed in control (Fig. 2B–F). Cell death assay using Sytox Green showed that cell death was dose-dependent on the concentration of H_2O_2 in both FECD-JPN and FECD-EUR, which was significantly higher than that of normal immortalized CECs and control iPSC-derived CECs (Fig. 2G). Cell death in FECD by H_2O_2 was significantly suppressed with the antioxidant NAC (Fig. 2H and I). Next, intracellular ROS level was measured by CellROX green staining. Treatment with 600 μM H_2O_2 for 4 h significantly increased fluorescence intensity only in FECD groups, which was reduced with NAC (Fig. 2J and K). These results indicate that induced CECs from FECD patients were more vulnerable to oxidative stress compared to control.

3.3. PARP-1, PAR and AIF upregulation in FECD

Western blotting showed that the amount of PAR polymer was higher in FECD than in control (Fig. 3A). Immunostaining of PAR polymer also confirmed cytoplasmic PAR accumulation in FECD (Fig. 3B). PARP-1 and AIF in the nuclear fraction were upregulated in FECD compared to control (Fig. 3C). Consistent with the findings in western blotting, AIF was observed in the nucleus in FECD (Fig. 3D). Taken together, these findings indicate that FECD CECs may be prone to parthanatos.

3.4. PARP inhibitor rescued FECD cells from parthanatos

To further confirm the involvement of parthanatos in FECD, we examined the effect of the PARP inhibitor, PJ34. Cell death induced by H_2O_2 in FECD was rescued with PJ34 treatment (Fig. 4A). To examine the cell death types induced by H_2O_2 in our model, we also conducted cell death assay with pan-caspase inhibitor, Z-VAD-FMK. Cell death ratio was not significantly reduced with Z-VAD-FMK in FECD (Fig. 4B).

Furthermore, the number of γH2AX foci to nucleus ratio increased significantly with H_2O_2 in FECD groups but not in control (Fig. 4C and D). PJ34 treatment significantly decreased this ratio in FECD indicating that while DNA double strand breaks were not significantly different among groups at baseline, DNA damage level was significantly higher in FECD treated with H_2O_2 (Fig. 4C and D).

In parthanatos, PAR polymer accumulation causes mitochondrial depolarization. We monitored the changes in MMP using JC-10 staining. JC-10 accumulates in mitochondria as a polymer and emits red fluorescence under high MMP states, while in low MMP, JC-10 localizes in the cytoplasm as a monomer and emits green fluorescence. H_2O_2 treatment decreased the red to green ratio significantly which was rescued with PJ34 treatment in FECD (Fig. 4E and F).

$***p = 5.0 \times 10^{-8}$, CTRL H_2O_2 vs FECD-EUR H_2O_2 $**p = 8.8 \times 10^{-3}$, FECD-JPN vs FECD-JPN H_2O_2 $***p = 8.4 \times 10^{-11}$, FECD-JPN H_2O_2 vs FECD-JPN NAC + H_2O_2 $p = 0.72$, FECD-EUR vs FECD-EUR H_2O_2 $***p = 6.7 \times 10^{-5}$, FECD-EUR H_2O_2 vs FECD-EUR NAC + H_2O_2 $*p = 0.03$). High intensity indicates upregulated ROS level. Scale bars are 100 μm. All data are presented as the mean ± SD values. All experiments were repeated 3 times independently.

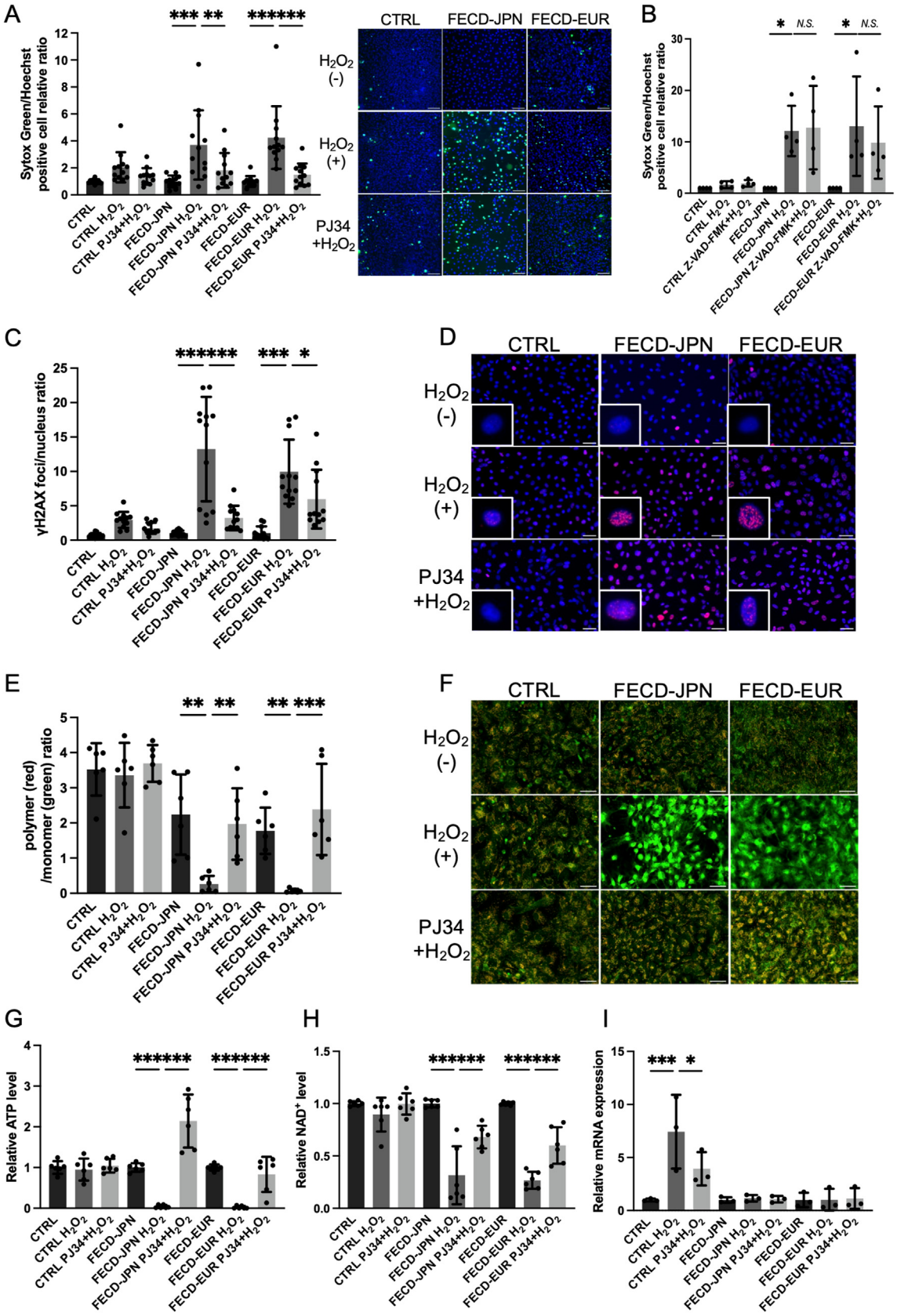

Fig. 4. PARP inhibitor, PJ34 rescued FECD cells from parthanatos. (A) Relative cell death ratio by H_2O_2 supplemented with PJ34 in each group and representative images ($n = 12$, FECD-JPN vs FECD-JPN H_2O_2 ***$p = 2.9 \times 10^{-5}$, FECD-JPN H_2O_2 vs FECD-JPN PJ34 + H_2O_2 **$p = 7.4 \times 10^{-3}$, FECD-EUR vs FECD-EUR H_2O_2 ***$p = 4.1 \times 10^{-7}$, FECD-EUR H_2O_2 vs FECD-EUR PJ34 + H_2O_2 ***$p = 1.9 \times 10^{-5}$). Scale bars are 100 μm. (B) Relative cell death ratio by H_2O_2 supplemented with pan-caspase inhibitor, Z-VAD-FMK in each

PARP-1 uses NAD^+ as a substrate and inhibits glycolysis, resulting in ATP depletion. ATP and NAD^+ levels were significantly decreased with H_2O_2 and rescued with PJ34 in FECD (Fig. 4G and H). In addition, the mRNA level of nicotinamide phosphoribosyltransferase (*NAMPT*), a rate-limiting enzyme during the process of NAD^+ production, was upregulated with H_2O_2 in control, while it did not change significantly in FECD (Fig. 4I). These results indicate that impairment of NAD^+ salvage pathway in FECD under oxidative stress may contribute to NAD^+ depletion, resulting in ATP decrease.

4. Discussion

Cell death is involved in the pathophysiology of FECD [3,11]. CECs have a limited proliferative potential *in vivo* [2], thus immortalized cell lines are often used for the analysis [9,12,25]. However, since cell death analysis using immortalized cell lines may not accurately reflect the pathophysiology, we used CECs induced from iPSCs in this study. iPSC-derived cells are widely used for disease modeling and drug development [32,33]. Cell death ratio with 600 μM H_2O_2 in control iPSC-derived CECs was significantly higher than that of normal immortalized CECs, suggesting that iPSC-derived CECs were more susceptible to cell death. iPSC-derived cells may still have limitations since age-dependent or environment-dependent epigenetic changes may be partially reprogrammed during iPSC generation [33,34]. However, by using a differentiation protocol tracing the development of CECs [26,30], we successfully captured the vulnerability of FECD cells to ROS compared with control. Although there is the possibility that pathological cell death pathways may be reprogrammed by iPSC induction, several studies have successfully used disease-specific iPSCs for drug screening using cell death as a parameter [35–38].

Once CECs die in FECD, the energy requirement to maintain corneal clarity cannot be compensated by cell proliferation and the energy requirements of the remaining CECs increase. This may induce oxidative stress [11], followed by a loss of mitochondrial membrane potential leading to further cell death [11]. Oxidative stress has been reported to induce CEC death by apoptosis and ferroptosis in FECD [13,16,17]. Our data suggest that parthanatos may also be a form of cell death involved in the pathogenesis of FECD. In parthanatos, PARP-1 and PAR overexpression, AIF translocation into the nucleus, and energy depletion such as NAD^+ and ATP are the key findings [21]. PARP-1 is also involved in apoptosis [39,40] and upregulation of PARP-1 in clinical samples from FECD patients has been reported previously [41]. However, to our knowledge, essential features of parthanatos such as PAR accumulation and AIF translocation to the nucleus and energy depletion have not been reported.

Parthanatos has been implicated in the pathogenesis of neurodegenerative diseases, ischemic diseases and cancer [42]. A significant amount of energy is required to dehydrate the cornea [1], and energy depletion by parthanatos may accelerate the vicious cycle of FECD pathogenesis. Several forms of cell death may contribute to the pathophysiology of the disease [15,21]. Both apoptosis and parthanatos are induced by oxidative stress and share some features in common such as mitochondrial depolarization, DNA damage, and chromatinolysis by γH2AX [15,43], all of which were all observed in our study. AIF translocates to the nucleus and interacts with γH2AX to induce chromatinolysis and large DNA fragmentation [43,44]. AIF translocation was not inhibited by caspase inhibitors, which is considered to be a unique feature of parthanatos [22,45]. In this study, microscopic examination revealed AIF in the nucleus in FECD, and the protein level of AIF was higher in FECD. In addition, the upregulated γH2AX foci to nucleus ratio, mitochondrial depolarization and energy depletion were reversed with a PARP inhibitor. Since pan-caspase inhibition did not significantly reduce cell death due to oxidative stress, our results suggest that parthanatos is mainly involved in FECD. It is not uncommon for more than one form of cell death are involved in the pathophysiology of disease [46]. Further studies are required to investigate the underlying mechanisms involved in the different forms of cell death in CECs of FECD.

Although it is still unclear as to how oxidative stress determines cell death by either apoptosis or parthanatos, NAD^+ salvage by NAMPT has been reported to be involved [47,48]. NAD^+ exists in both the cytoplasm and mitochondria, and under normal conditions, nuclear PARP-1 consumes only cytosolic NAD^+, which can be replenished by NAMPT [49]. In our study, control CECs expressed higher mRNA levels of *NAMPT* under H_2O_2 treatment, which may have allowed salvage of cytosolic NAD^+, but not in FECD CECs with lower *NAMPT* expression. Excessive consumption of NAD^+ under oxidative stress combined with weak recovery by NAMPT may play a role in the pathophysiology of FECD.

In addition to its role of regulating energy homeostasis [50], PARP-1 also plays an important role as a DNA damage sensor [51]. It is abundant in the nucleus where it regulates chromatin structure and transcription [52]. Mild upregulation of PARP-1 facilitates DNA repair, whereas excessive activation of PARP-1 triggers DNA fragmentation and cell death by parthanatos [51]. The extent of DNA damage by oxidative stress and the location of the activated domain of PARP-1 is thought to determine PARP-1 expression levels, but detailed mechanisms have not been elucidated [51]. Mild upregulation of PARP-1 contributes to DNA repair through replication, base excision repair and double-strand break repair [51]. In FECD, the mRNA level of PARP-1 was reported to be neither up- nor downregulated in the corneal endothelium and Descemet's membrane samples [53]. In our study, nuclear PARP-1 and AIF protein levels were higher than control, suggesting that nuclear PARP-1 expression may be excessive, leading to parthanatos.

group ($n = 4$, FECD-JPN vs FECD-JPN H_2O_2 $*p = 0.03$, FECD-EUR vs FECD-EUR H_2O_2 $*p = 0.01$). (C, D) The number of foci to nucleus ratio of γH2AX by H_2O_2 supplemented with PJ34 and representative images ($n = 12$, FECD-JPN vs FECD-JPN H_2O_2 $***p = 2.6 \times 10^{-13}$, FECD-JPN H_2O_2 vs FECD-JPN PJ34 + H_2O_2 $***p = 6.4 \times 10^{-10}$, FECD-EUR vs FECD-EUR H_2O_2 $***p = 2.7 \times 10^{-8}$, FECD-EUR H_2O_2 vs FECD-EUR PJ34 + H_2O_2 $*p = 0.03$). Foci is observed at the site of DNA double-strand breaks. Scale bars are 50 μm. (E, F) Relative MMP ratio by H_2O_2 supplemented with PJ34 in each group and representative images ($n = 6$, FECD-JPN vs FECD-JPN H_2O_2 $**p = 1.2 \times 10^{-3}$, FECD-JPN H_2O_2 vs FECD-JPN PJ34 + H_2O_2 $**p = 6.7 \times 10^{-3}$, FECD-EUR vs FECD-EUR H_2O_2 $**p = 6.9 \times 10^{-3}$, FECD-EUR H_2O_2 vs FECD-EUR PJ34 + H_2O_2 $***p = 1.3 \times 10^{-4}$). Ratio of red to green fluorescence intensity is decreased in low MMP. Scale bars are 50 μm. (G) Relative intracellular ATP levels by H_2O_2 supplemented with PJ34 in each group ($n = 6$, FECD-JPN vs FECD-JPN H_2O_2 $***p = 4.4 \times 10^{-6}$, FECD-JPN H_2O_2 vs FECD-JPN PJ34 + H_2O_2 $***p = 2.0 \times 10^{-15}$, FECD-EUR vs FECD-EUR H_2O_2 $***p = 3.1 \times 10^{-6}$, FECD-EUR H_2O_2 vs FECD-EUR PJ34 + H_2O_2 $***p = 9.6 \times 10^{-5}$). (H) Relative intracellular NAD^+ levels by H_2O_2 supplemented with PJ34 in each group ($n = 6$, FECD-JPN vs FECD-JPN H_2O_2 $***p = 2.0 \times 10^{-10}$, FECD-JPN H_2O_2 vs FECD-JPN PJ34 + H_2O_2 $***p = 2.1 \times 10^{-4}$, FECD-EUR vs FECD-EUR H_2O_2 $***p = 2.7 \times 10^{-11}$, FECD-EUR H_2O_2 vs FECD-EUR PJ34 + H_2O_2 $***p = 7.8 \times 10^{-4}$). (I) Relative mRNA expression of *NAMPT* by H_2O_2 supplemented with PJ34 in each group ($n = 3$, $***p = 8.9 \times 10^{-5}$, $*p = 0.03$). All data are presented as the mean ± SD values. All experiments were repeated 3 times independently, except for (B) (4 times).

5. Conclusions

This study showed that the non-apoptotic cell death parthanatos may contribute to the pathogenesis of FECD using induced CECs from FECD patients. The PARP-1 inhibitor, PJ34, rescued the characteristic phenotypes of parthanatos, suggesting that targeting the downstream pathways of parthanatos may be a potential avenue for the therapy of FECD.

Ethics approval and consent to participate

All experiments were approved by the Institutional Review Board of Keio University School of Medicine Ethics Committee (approval number: 20130221).

Consent for publication

Written and informed consent was obtained from patients.

Availability of data and materials

The datasets generated and/or analyzed during the current study are available from the corresponding author on reasonable request.

Authors' contributions

SS (Saki Sakakura), EI and SS (Shigeto Shimmura) designed the study. RY and NF generated iPSCs. SS (Saki Sakakura) performed characterization of iPSCs and CECs, oxidative stress and cell death assays and data analysis. EI, SH, HO and SS (Shigeto Shimmura) supervised this project. The manuscript was written by SS (Saki Sakakura). All authors contributed to the final editing and approval of the manuscript.

Declaration of competing interest

The authors declare that they have no competing interests.

Acknowledgements

We thank the members of the Laboratory of Corneal Cell Biology for their kind assistance. We also thank JSR-Keio University Medical and Chemical Innovation Center (JKiC), Etsuko Sugai, Satoru Yoshida, Hideyuki Miyashita and the Collaborative Research Resources, Keio University School of Medicine, for technical assistance and general support. This work was supported by Grants-in-Aid for Scientific Research from Japan Society for the Promotion of Science (JSPS) to SS (Shigeto Shimmura) (Grant Number: KAKENHI 19K09978); by Grants-in-Aid for Scientific Research from Japan Society for the Promotion of Science (JSPS) to EI and KT (Grant Number: KAKENHI 17H04353); by Grant-in-Aid by JKiC/JSR (Academic Development Project 2021) to EI; by Kobayashi Foundation Research Fund to EI; by Keio University Medical Science Fund to EI; by PRESTO, Japan Science and Technology Agency to NF (Grant Number: JPMJPR09F7) and by the Keio University Doctorate Student Grant-in-Aid Program from Ushioda Memorial Fund to SS (Saki Sakakura).

Appendix A. Supplementary data

Supplementary data to this article can be found online at https://doi.org/10.1016/j.reth.2023.11.001.

References

[1] Bonanno JA. Molecular mechanisms underlying the corneal endothelial pump. Exp Eye Res 2012;95:2–7.
[2] Joyce NC. Proliferative capacity of the corneal endothelium. Prog Retin Eye Res 2003;22:359–89.
[3] Ong Tone S, Kocaba V, Bohm M, Wylegala A, White TL, Jurkunas UV. Fuchs endothelial corneal dystrophy: the vicious cycle of Fuchs pathogenesis. Prog Retin Eye Res 2021;80:100863.
[4] Gain P, Jullienne R, He Z, Aldossary M, Acquart S, Cognasse F, et al. Global survey of corneal transplantation and eye banking. JAMA Ophthalmol 2016;134:167–73.
[5] Aiello F, Gallo Afflitto G, Ceccarelli F, Cesareo M, Nucci C. Global prevalence of Fuchs endothelial corneal dystrophy (FECD) in adult population: a systematic review and meta-analysis. J Ophthalmol 2022;2022:3091695.
[6] Jurkunas UV. Fuchs endothelial corneal dystrophy through the prism of oxidative stress. Cornea 2018;37(Suppl 1):S50–4.
[7] Jurkunas UV, Bitar MS, Funaki T, Azizi B. Evidence of oxidative stress in the pathogenesis of Fuchs endothelial corneal dystrophy. Am J Pathol 2010;177:2278–89.
[8] Lovatt M, Kocaba V, Hui Neo DJ, Soh YQ, Mehta JS. Nrf2: a unifying transcription factor in the pathogenesis of Fuchs' endothelial corneal dystrophy. Redox Biol 2020;37:101763.
[9] Okumura N, Kitahara M, Okuda H, Hashimoto K, Ueda E, Nakahara M, et al. Sustained activation of the unfolded protein response induces cell death in Fuchs' endothelial corneal dystrophy. Invest Ophthalmol Vis Sci 2017;58:3697–707.
[10] Kumar V, Jurkunas UV. Mitochondrial dysfunction and mitophagy in Fuchs endothelial corneal dystrophy. Cells 2021:10.
[11] Methot SJ, Proulx S, Brunette I, Rochette PJ. Chronology of cellular events related to mitochondrial burnout leading to cell death in Fuchs endothelial corneal dystrophy. Sci Rep 2020;10:5811.
[12] Katikireddy KR, White TL, Miyajima T, Vasanth S, Raoof D, Chen Y, et al. NQO1 downregulation potentiates menadione-induced endothelial-mesenchymal transition during rosette formation in Fuchs endothelial corneal dystrophy. Free Radic Biol Med 2018;116:19–30.
[13] Halilovic A, Schmedt T, Benischke AS, Hamill C, Chen Y, Santos JH, et al. Menadione-induced DNA damage leads to mitochondrial dysfunction and fragmentation during rosette formation in Fuchs endothelial corneal dystrophy. Antioxidants Redox Signal 2016;24:1072–83.
[14] Kim EC, Meng H, Jun AS. N-Acetylcysteine increases corneal endothelial cell survival in a mouse model of Fuchs endothelial corneal dystrophy. Exp Eye Res 2014;127:20–5.
[15] Tang D, Kang R, Berghe TV, Vandenabeele P, Kroemer G. The molecular machinery of regulated cell death. Cell Res 2019;29:347–64.
[16] Li QJ, Ashraf MF, Shen DF, Green WR, Stark WJ, Chan CC, et al. The role of apoptosis in the pathogenesis of Fuchs endothelial dystrophy of the cornea. Arch Ophthalmol 2001;119:1597–604.
[17] Lovatt M, Adnan K, Kocaba V, Dirisamer M, Peh GSL, Mehta JS. Peroxiredoxin-1 regulates lipid peroxidation in corneal endothelial cells. Redox Biol 2020;30:101417.
[18] David KK, Andrabi SA, Dawson TM, Dawson VL. Parthanatos, a messenger of death. Front Biosci 2009;14:1116–28.
[19] Wang Y, Dawson VL, Dawson TM. Poly(ADP-ribose) signals to mitochondrial AIF: a key event in parthanatos. Exp Neurol 2009;218:193–202.
[20] Kam TI, Mao X, Park H, Chou SC, Karuppagounder SS, Umanah GE, et al. Poly(ADP-ribose) drives pathologic alpha-synuclein neurodegeneration in Parkinson's disease. Science 2018;362.
[21] Fatokun AA, Dawson VL, Dawson TM. Parthanatos: mitochondrial-linked mechanisms and therapeutic opportunities. Br J Pharmacol 2014;171:2000–16.
[22] Liu L, Li J, Ke Y, Zeng X, Gao J, Ba X, et al. The key players of parthanatos: opportunities for targeting multiple levels in the therapy of parthanatos-based pathogenesis. Cell Mol Life Sci 2022;79:60.
[23] Zhou Y, Liu L, Tao S, Yao Y, Wang Y, Wei Q, et al. Parthanatos and its associated components: promising therapeutic targets for cancer. Pharmacol Res 2021;163:105299.
[24] Wang Y, An R, Umanah GK, Park H, Nambiar K, Eacker SM, et al. A nuclease that mediates cell death induced by DNA damage and poly(ADP-ribose) polymerase-1. Science 2016;354.
[25] Kim EC, Toyono T, Berlinicke CA, Zack DJ, Jurkunas U, Usui T, et al. Screening and characterization of drugs that protect corneal endothelial cells against unfolded protein response and oxidative stress. Invest Opthalmology Visual Sci 2017;58:892.
[26] Hatou S, Shimmura S. Review: corneal endothelial cell derivation methods from ES/iPS cells. Inflamm Regen 2019;39:19.
[27] Lau LC, Ma L, Young AL, Rong SS, Jhanji V, Brelen ME, et al. Association of common variants in TCF4 and PTPRG with Fuchs' corneal dystrophy: a systematic review and meta-analysis. PLoS One 2014;9:e109142.
[28] Afshari NA, Igo Jr RP, Morris NJ, Stambolian D, Sharma S, Pulagam VL, et al. Genome-wide association study identifies three novel loci in Fuchs endothelial corneal dystrophy. Nat Commun 2017;8:14898.
[29] Seki T, Yuasa S, Oda M, Egashira T, Yae K, Kusumoto D, et al. Generation of induced pluripotent stem cells from human terminally differentiated circulating T cells. Cell Stem Cell 2010;7:11–4.

[30] Zhao JJ, Afshari NA. Generation of human corneal endothelial cells via in vitro ocular lineage restriction of pluripotent stem cells. Invest Ophthalmol Vis Sci 2016;57:6878–84.
[31] ImageJ WSR. U.S. National Institutes of Health. Bethesda, MD, USA, http://rsb.info.nih.gov/ij/. 2009.
[32] Nicholson MW, Ting CY, Chan DZH, Cheng YC, Lee YC, Hsu CC, et al. Utility of iPSC-derived cells for disease modeling, drug development, and cell therapy. Cells 2022:11.
[33] Okano H, Morimoto S. iPSC-based disease modeling and drug discovery in cardinal neurodegenerative disorders. Cell Stem Cell 2022;29:189–208.
[34] Kim K, Zhao R, Doi A, Ng K, Unternaehrer J, Cahan P, et al. Donor cell type can influence the epigenome and differentiation potential of human induced pluripotent stem cells. Nat Biotechnol 2011;29:1117–9.
[35] Fujimori K, Ishikawa M, Otomo A, Atsuta N, Nakamura R, Akiyama T, et al. Modeling sporadic ALS in iPSC-derived motor neurons identifies a potential therapeutic agent. Nat Med 2018;24:1579–89.
[36] Sharma R, George A, Nimmagadda M, Ortolan D, Karla BS, Qureshy Z, et al. Epithelial phenotype restoring drugs suppress macular degeneration phenotypes in an iPSC model. Nat Commun 2021;12:7293.
[37] Cai H, Gong J, Abriola L, Hoyer D, Nyscf Global Stem Cell Array T, Noggle S, et al. High-throughput screening identifies compounds that protect RPE cells from physiological stressors present in AMD. Exp Eye Res 2019;185:107641.
[38] Gu M, Donato M, Guo M, Wary N, Miao Y, Mao S, et al. iPSC-endothelial cell phenotypic drug screening and in silico analyses identify tyrphostin-AG1296 for pulmonary arterial hypertension. Sci Transl Med 2021:13.
[39] Mashimo M, Onishi M, Uno A, Tanimichi A, Nobeyama A, Mori M, et al. The 89-kDa PARP1 cleavage fragment serves as a cytoplasmic PAR carrier to induce AIF-mediated apoptosis. J Biol Chem 2021;296:100046.
[40] Chaitanya GV, Steven AJ, Babu PP. PARP-1 cleavage fragments: signatures of cell-death proteases in neurodegeneration. Cell Commun Signal 2010;8:31.
[41] Wang X, Dong C, Zhou Q, Duan H, Zou D, Gong Y, et al. Poly(ADP-ribose) polymerase inhibitor PJ34 protects against UVA-induced oxidative damage in corneal endothelium. Apoptosis 2021;26:600–11.
[42] Huang P, Chen G, Jin W, Mao K, Wan H, He Y. Molecular mechanisms of parthanatos and its role in diverse diseases. Int J Mol Sci 2022;23.
[43] Baritaud MBH, Lorenzo HK, Krantic S, Susin SA. Histone H2AX: the missing link in AIF-mediated caspase-independent programmed necrosis. Cell Cycle 2010;15(9):3186–93.
[44] Artus C, Boujrad H, Bouharrour A, Brunelle MN, Hoos S, Yuste VJ, et al. AIF promotes chromatinolysis and caspase-independent programmed necrosis by interacting with histone H2AX. EMBO J 2010;29:1585–99.
[45] Daugas E, Susin SA, Zamzami N, Ferri KF, Irinopoulou T, Larochette N, et al. Mitochondrio-nuclear translocation of AIF in apoptosis and necrosis. Faseb J 2000;14:729–39.
[46] Vanden Berghe T, Linkermann A, Jouan-Lanhouet S, Walczak H, Vandenabeele P. Regulated necrosis: the expanding network of non-apoptotic cell death pathways. Nat Rev Mol Cell Biol 2014;15:135–47.
[47] Nishida T, Naguro I, Ichijo H. NAMPT-dependent NAD(+) salvage is crucial for the decision between apoptotic and necrotic cell death under oxidative stress. Cell Death Dis 2022;8:195.
[48] Eguchi Y, Shimizu S, Tsujimoto Y. Intracellular ATP levels determine cell death fate by apoptosis or necrosis. Cancer Res 1997;57:1835–40.
[49] Alano CC, Tran A, Tao R, Ying W, Karliner JS, Swanson RA. Differences among cell types in NAD(+) compartmentalization: a comparison of neurons, astrocytes, and cardiac myocytes. J Neurosci Res 2007;85:3378–85.
[50] Andrabi SA, Umanah GK, Chang C, Stevens DA, Karuppagounder SS, Gagne JP, et al. Poly(ADP-ribose) polymerase-dependent energy depletion occurs through inhibition of glycolysis. Proc Natl Acad Sci U S A 2014;111:10209–14.
[51] Wang Y, Luo W, Wang Y. PARP-1 and its associated nucleases in DNA damage response. DNA Repair 2019;81:102651.
[52] Krishnakumar R, Kraus WL. The PARP side of the nucleus: molecular actions, physiological outcomes, and clinical targets. Mol Cell 2010;39:8–24.
[53] Ashraf S, Deshpande N, Vasanth S, Melangath G, Wong RJ, Zhao Y, et al. Dysregulation of DNA repair genes in Fuchs endothelial corneal dystrophy. Exp Eye Res 2023;231:109499.